Bioorganic & Medicinal Chemistry 16 (2008) 7337–7346

Contents lists available at ScienceDirect

Bioorganic & Medicinal Chemistry

journal homepage: www.elsevier.com/locate/bmc

Functionalized pyrrolidine inhibitors of human type II α-mannosidases as anti-cancer agents: Optimizing the fit to the active site

Hélène Fiaux [a], Douglas A. Kuntz [b], Daniella Hoffman [b], Robert C. Janzer [c], Sandrine Gerber-Lemaire [a,*], David R. Rose [b,*], Lucienne Juillerat-Jeanneret [c,*]

[a] Laboratory of Glycochemistry and Asymmetric Synthesis, Ecole Polytechnique Fédérale de Lausanne (EPFL), CH-1015 Lausanne, Switzerland
[b] Department of Medical Biophysics, University of Toronto and Division of Cancer Genomics and Proteomics, Ontario Cancer Institute, Toronto, Ont., Canada M5G 1L7
[c] University Institute of Pathology, CHUV, Rue du Bugnon 25, CH-1011 Lausanne, Switzerland

ARTICLE INFO

Article history:
Received 22 April 2008
Revised 4 June 2008
Accepted 11 June 2008
Available online 14 June 2008

Keywords:
α-Mannosidase inhibitors
X-ray crystallography
Glioblastoma
Anti-cancer agents

ABSTRACT

Refining the chemical structure of functionalized pyrrolidine-based inhibitors of Golgi α-mannosidase II (GMII) to optimize binding affinity provided a lead molecule that demonstrated nanomolar competitive inhibition of α-mannosidases II and an optimal fit in the active site of *Drosophila* GMII by X-ray crystallography. Esters of this lead compound also inhibited the growth of human glioblastoma and brain-derived endothelial cells more than the growth of non-tumoral human fibroblasts, suggesting their potential for anti-cancer therapy.

1. Introduction

Changes in the glycosylation pattern of cellular glycoproteins are common features of human cancer and influence tumor progression[1–18] suggesting that inhibitors of selected glycosidases may control cancer.[5–11] The assembly of the oligosaccharide chain of cellular glycoproteins is initiated in the endoplasmic reticulum on the nascent protein being synthesized on the ribosomes. At that stage all glycoproteins bear the same carbohydrate structure. Following trimming by α-glucosidases I and II and α-mannosidase I the nascent glycoprotein is transported to the cis Golgi. In the medial Golgi, α-mannosidase II removes the α1,3-Man and α1,6-Man to form $GlcNAcMan_3$ $(GlcNAc)_2$-protein. Then other carbohydrate molecules can be added to this core producing diversity in glycoproteins. Further metabolism/catabolism of glycoproteins[12,13] is also observed in the cytosol and the lysosomes, involving several glycosidases.

Our previous approaches using functionalized glycomers[14] or functionalized pyrrolidines[15–21] and results from others using swainsonine (Scheme 1), a 4-amino-4-deoxy-mannofuranoside natural inhibitor of Golgi α-mannosidases of type II (GMII),[11,13,22–37] suggested that inhibiting cellular mannosidases, in particular GMII, represents potential innovative methods for drug development in human cancer. However, the poor cellular bioavailability of swainsonine, its side effects, as well as the undesired co-inhibition of lysosomal enzymes has resulted in the search for new, more selective, α-mannosidase inhibitors. Recently, we reported that 3,4-dihydroxy-pyrrolidin-2-yl derivatives are selective and competitive inhibitors of α-mannosidase from jack bean,[15–18] and we also demonstrated promising anti-proliferative activities on human glioblastoma and melanoma cells for the cell-permeant ester of this compound.[19–21] A high resolution structure of the co-crystal of *Drosophila* GMII (dGMII) with our first lead[19] allowed the elucidation of its binding in the active site of dGMII.[38] The hydroxyl moieties of the pyrrolidine ring made tight interactions with the active site zinc, involved in substrate binding. Trp95 displayed two types of pi interactions: the commonly seen stacked interaction with the five membered ring and an unusual T-shaped interaction with the center of the aromatic ring. Nitrogen atoms and the terminal oxygen (O9) provided several polar interactions. Interestingly and in contrast to other structures of dGMII:inhibitor complexes, there is no hydroxyl group occupying the space between Asp472 and Tyr727. This information was the basis of refining the structures of our molecules. We hypothesized that the introduction of polar substituents at the C(5) position of the pyrrolidine ring of our first lead may induce additional interactions with these two residues of the enzyme active site. For that purpose, replacement of the pyrrolidine moiety by a pyrrolidinone system

* Corresponding authors. Tel.: +41 21 693 93 72; fax: +41 21 693 93 55 (S.G.-L.); tel.: +416 581 7537; fax: +416 581 7562 (D.R.R.); tel.: +41 21 314 7173; fax: +41 21 314 7115 (L.J.-J.).
E-mail addresses: Sandrine.Gerber@epfl.ch (S. Gerber-Lemaire), drose@oci.utoronto.ca (D.R. Rose), lucienne.juillerat@chuv.ch (L. Juillerat-Jeanneret).

0968-0896/$ - see front matter © 2008 Elsevier Ltd. All rights reserved.
doi:10.1016/j.bmc.2008.06.021

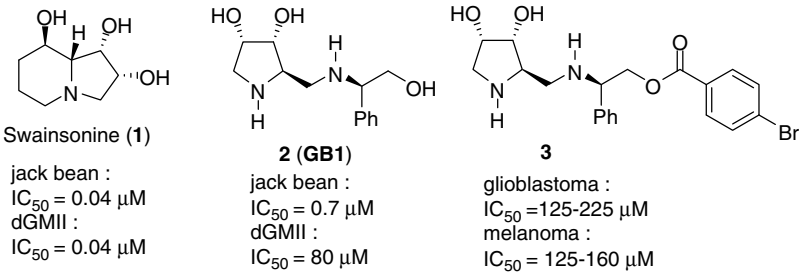

Scheme 1. Swainsonine and the previous pyrrolidine derivatives as anti-cancer agents.

was envisaged. We report here the synthesis of these new inhibitors, and their kinetic, structural, and biological evaluations.

2. Results

2.1. Chemical syntheses

The synthesis (Scheme 2) started from 5-oxo-L-proline, which was converted into the primary alcohol **4** with 84% yield. Protection as a *tert*-butyldimethylsilyl ether was followed by introduction of a *tert*-butyl carbamate (**5**) or a methyl group (**6**) on the nitrogen atom. A three step procedure[39] involving conversion into the corresponding 3-selenopyrrolidinone followed by oxidative elimination of the phenylselenyl moiety and dihydroxylation of the resulting enone, in the presence of a catalytic amount of osmium tetroxide, provided diols **7** and **8** with 43 and 41% yield (3 steps), respectively. Protection of the hydroxyl groups as acetonides allowed, after desilylation, oxidation of the primary alcohol and reductive amination in the presence of D-(−)-α-phenylglycinol and sodium triacetoxyborohydride for in situ reduction of the intermediate imines. A final acidic treatment afforded the 3,4-dihydroxy pyrrolidinone derivatives **11** and **12** in 12 and 28% yield (4 steps), respectively. The same sequence of reactions was performed with 4-bromobenzoylphenyl glycinol to deliver the ester derivatives **13** and **14**. The detailed procedures and the characterization of the compounds are provided as Supplemental data.

2.2. Inhibition of jack bean and *Drosophila* α-mannosidases

The inhibitory potential of compounds **11** and **12** toward α-mannosidases from jack bean and *Drosophila* was determined and compared with the previously reported lead pyrrolidine derivative **2** and swainsonine **1** (Table 1). All inhibitors were competitive inhibitors. Replacement of the pyrrolidine moiety in **2** by a pyrrolidinone system in **11** resulted in a significant decrease of the inhibitory potency toward jack bean α-mannosidase. However, substitution of the lactam moiety by a methyl group in **12** induced a clear improvement of the inhibition potency of jack bean enzyme and **12** was as efficient as swainsonine for the inhibition of this enzyme. The inhibition of *Drosophila* GMII (dGMII) by pyrrolidine **2** was very modest, while pyrrolidinone derivatives considerably improved the inhibition. Whereas remaining 15 times less potent than swainsonine, derivative **12** demonstrated a 67-fold improvement from our previous lead **2**.[19]

2.3. Crystal structures

The structures of **11** and **12** complexed with dGMII were solved to 1.08 and 1.74 Å, respectively, and provided a clear view of the binding mode of the inhibitors into the active site of the enzyme. Supplemental Table S1 provides data collection and refinement statistics. Very clear electron density was obtained for the entire inhibitors **11** and **12** in the enzyme active site

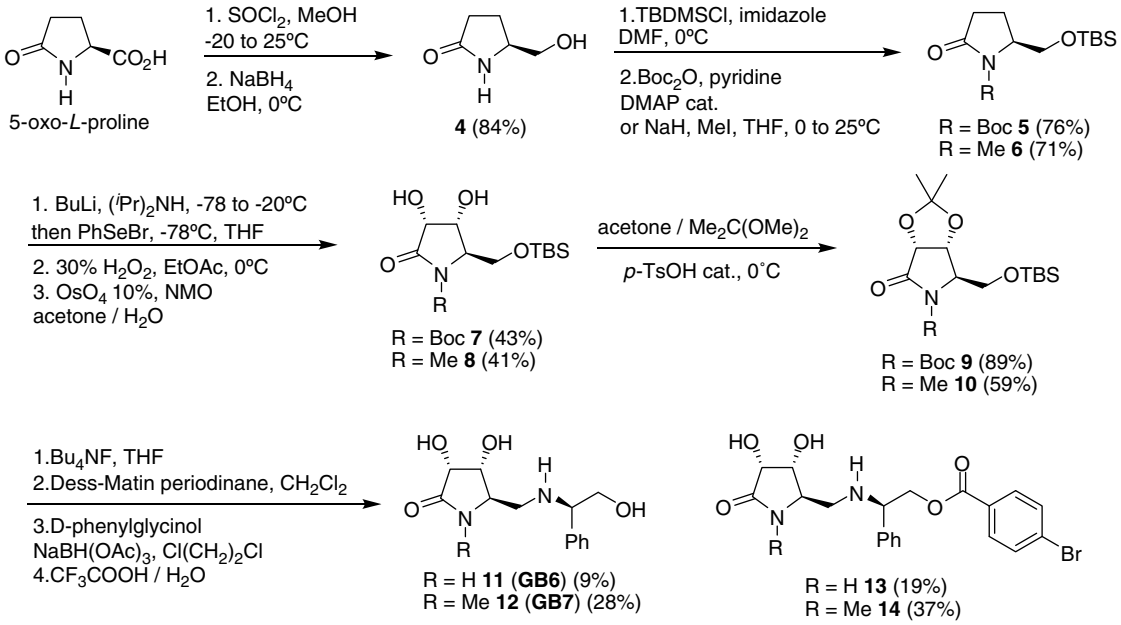

Scheme 2. Synthesis of 3,4-dihydroxypyrrolidinone derivatives.

Table 1
Inhibition of α-mannosidases from jack bean and dGMII by swainsonine and the pyrrolidine derivatives

Compound	α-Mannosidase from jack bean	dGMII
1 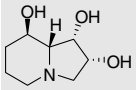	[a]K_i = 155 nM (C)	[b]K_i = 20 nM
2 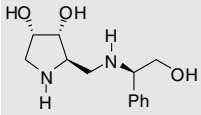	[a]K_i = 135 nM (C)	[b]K_i = 67 μM
11 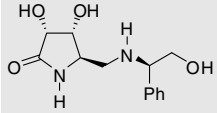	[a]K_i = 4 μM (C)	[b]K_i = 22 μM
12 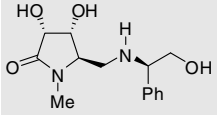	[a]K_i = 206 nM (C)	[b]K_i = 1 μM

Jack bean or dGMII α-mannosidases were exposed to increasing concentrations of the inhibitors under investigation and K_i were determined using 4-nitrophenyl-α-D-mannopyranoside as substrate at 37 °C or 20 °C.
(C), competitive inhibition.
[a] Determined at 37 °C.
[b] Determined at 20 °C.

(Fig. 1A), although the density of the pyrrolidine ring, which is bound to the zinc, was better defined than that of the aromatic ring. As previously seen for **2** (Supplemental Figure S1, adapted from[38]) the inhibitor phenyl ring made a T-shaped pi interaction with Trp95. Superimposing the structures of the dGMII:**12** complex solved here with the previously solved dGMII:**2** complex (PDB:2F18) showed that the two phenyl rings overlap quite closely (Fig. 2B). The presence of the carbonyl group on the pyrrolidine ring in **11** and **12** allows the formation of new hydrogen bonds between the carbonyl oxygen and both Asp472, and Tyr727 (Fig. 1B). Comparable hydrogen bonds were not seen in the dGMII:**2** structure. The presence of the oxo moiety enforces the planarity of the pyrrolidine ring. However, the bound conformation of the pyrrolidine ring is clearly different in the two structures (Figs. 1b and 2B). The N1–C2 bond demonstrates partial double bonded nature, its length refined to 1.32 Å, rather than 1.48 Å expected for a C-N single bond. The nitrogen atom of the five membered ring of the pyrrolidine inhibitor **2** presents a p*K*a of 8.17 (data not shown) and is thus protonated at the pH of the experiments, leading to a strong interaction with the Asp204 residue of the enzyme (2.81 Å). For the non-protonable *N*-methyl pyrrolidinone **12**, this interaction is lost and the distance between the nitrogen atom and the Asp204 residue increases to 3.42 Å. Nevertheless, two strong additional interactions are gained between the oxo moiety of the inhibitor and the Asp472 (2.60 Å) and Tyr727 (2.74 Å) residues. Moreover, of the *N*-methyl group enters into the hydrophobic pocket of the enzyme binding site formed by Phe206, Trp415, and Tyr727, which confers to the inhibitor **12** an increased affinity for dGMII. A direct comparison of the conformations of the pyrrolidine ring in **12** with **2**, swainsonine and mannostatin (another known inhibitor of dGMII [40]) is also made (Fig. 2). Overlaying the structure of bound **12** with the potent inhibitors mannostatin and swainsonine shows that the positions of the hydroxyl groups (or carbonyl group in **12**) are all very similar (Fig. 2C and D). All the distances of the interaction between these residues of the inhibitors and the residues of dGMII to which they bind (zinc, Asp92, Asp204, Asp472, and Tyr727) are very comparable (Supplemental Table S2). Additional interactions occur with Tyr269, Asp340, Asp341, which are not observed with the smaller α-mannosidase inhibitors mannostatin and swainsonine (Fig. 1B and Supplemental Table S2). The N-methyl group of **12** which differentiates it from **11** is close to the position of the thio-methyl group of mannostatin and the C6 group of swainsonine (Fig. 2C and D). This N-methyl group is pointing toward a hydrophobic pocket of the enzyme active site composed of Phe206, Trp415 and Tyr727 (Fig. 1B). This supplementary hydrophobic interaction formed by the methyl group with the hydrophobic pocket may be responsible for the increased inhibitory efficacy of **12** compared to **11**. The structure of the dGMII:**11** complex indicates the presence of a water-mediated interaction between the backbone carbonyl of Arg876 and the amino group of the pyrrolidine ring. This water molecule is displaced by the presence of the *N*-methyl group and undergoes a significant movement (Fig. 1B). The loss of this water-mediated interaction is not detrimental to the inhibitory activity of the compound and from the inhibition constants it can be inferred that the hydrophobic interactions induced by the presence of the methyl group are obviously preferred.

2.4. Inhibition of α-mannosidase II of human glioblastoma and brain-derived endothelial cells

Both tumor cells and angiogenic endothelial cells of human glioblastoma may be potential targets for α-mannosidase inhibitors to control human glioblastoma progression. Based on this information we evaluated the inhibition by our derivatives of α-mannosidases II from LN18 and LNZ308 human glioblastoma cell lines[19,41] and HCEC human brain-derived angiogenic endothelial cells.[14,41] Derivatives **1**, **2**, and **12** were first evaluated on α-mannosidase II activity extracted from human LN18 and LNZ308 glioblastoma cells and brain-derived HCEC endothelial cells, and K_M, IC_{50}, and K_i were determined (Table 2). Inhibitor **2**[19] showed a moderate inhibitory potency on α-mannosidases from all cell extracts. Introduction of an oxo moiety at the C(5) position in **11** of the five-membered ring did not change the inhibition significantly. The *N*-methyl pyrrolidinone compound **12** displayed potent inhibition of α-mannosidases extracted from LNZ308, LN18, and HCEC cells. The derivatization of **11** and **12** into their 4-bromo-benzoate esters **13** and **14**, respectively, induced a decrease of the inhibitory potency (Table 2), similarly to what was observed with our first lead **2** and its 4-bromobenzoate ester **3**[19] (structures in Scheme 1), as expected by the loss of interactions between the primary alcohol and residues of the active site of the enzyme. Still, a moderate amount of inhibition was observed, suggesting partial cleavage by cellular esterases to release the free primary alcohol.

2.5. Inhibition of the growth of human glioblastoma cells, proliferating endothelial cells, and fibroblasts

As previously reported for **1** and our first lead compound **2**,[19] the non-esterified derivatives **11** and **12** did not inhibit the growth of human glioblastoma cells and brain-derived endothelial cells (Supplemental Table S3). Whereas the 4-bromobenzoate derivative **13** demonstrated a modest 51 and 59% growth inhibition at 300 μM of LNZ308 and LN18 cell lines, respectively, the growth inhibition of HCEC cells (85% at 300 μM) was more efficient. Compound **14** was more potent than **13** and presented a time- and con-

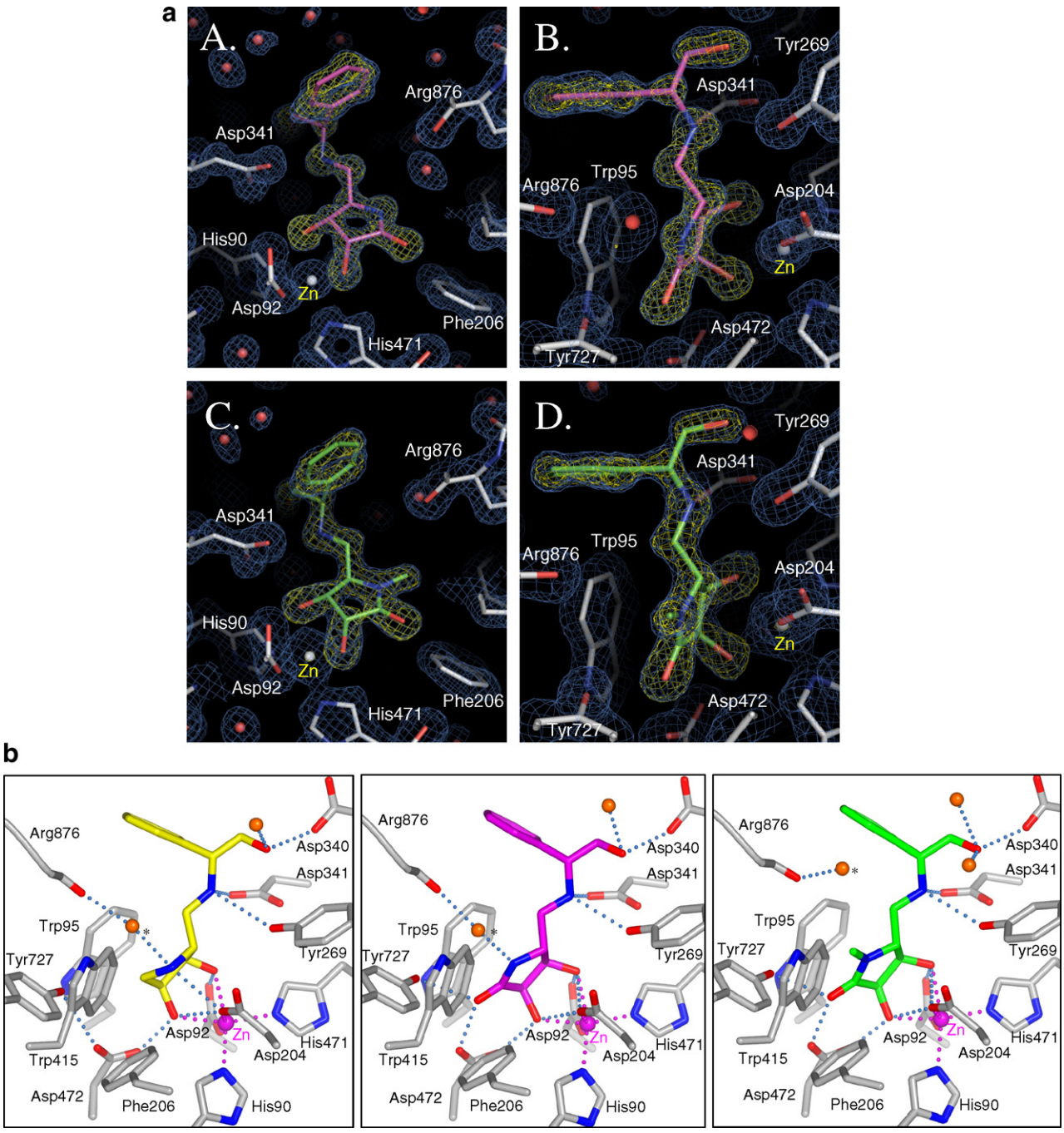

Figure 1. Interactions of the α-mannosidase inhibitors with the active site of dGMII. (a) Electron density of the active site of dGMII complexes with **11** (A,B) or **12** (C,D). Views A and C are approximately from the position of Trp95 which forms a lid on the binding site pocket, B and D are after an approximate 100 degree rotation. Maps are simulated-annealing composite omit maps. The $F_{obs} - F_{calc}$ map shown in yellow is contoured at 5 sigma, the 2 $F_{obs} - F_{calc}$ map (blue) is contoured at 1.4 sigma. The compound **11** is colored magenta and **12** is colored green. (b) Comparison of pyrrolidine analogs in the active site of dGMII. Residues interacting with distances of less than 3.2 Å are indicated. The left panel illustrates the previously described **2** (PDB: 2F18), the middle panel the **11** structure and the right panel **12**. The active site zinc atom is shown as a magenta sphere and water molecules are represented as orange spheres. The water molecule whose position is altered significantly by the incorporation of the amino-methyl group is indicated with an asterisk.

centration-dependent inhibition of the growth of all cell lines, producing complete inhibition at 300 μM within 24 h, comparable to derivative **3**.[19] A dose–response evaluation of the anti-proliferative effects of the best derivative **14** achieved IC_{50} values of 175 μM and 145 μM in LNZ308 and LN18 cells, respectively (Fig. 3A). In HCEC cells, the inhibition profile was slightly different and the IC_{50} was 100 μM. To evaluate the cell selectivity for tumor and tumor-associated cells of our new lead, human pulmonary and skin fibroblasts were exposed to **14**, and only very modest growth inhibition was observed, much lower than the growth inhibition induced by our previous lead **3**[19] (Fig. 3B).

2.6. Effects of α-mannosidase inhibitor 14 on human glioblastoma cells and proliferating endothelial cell functions

To get insights into the mode of action of derivative **14**, we evaluated the expression of binding sites for the lectin LcH, recognizing terminal mannoses, in human LNZ308 glioblastoma cells exposed

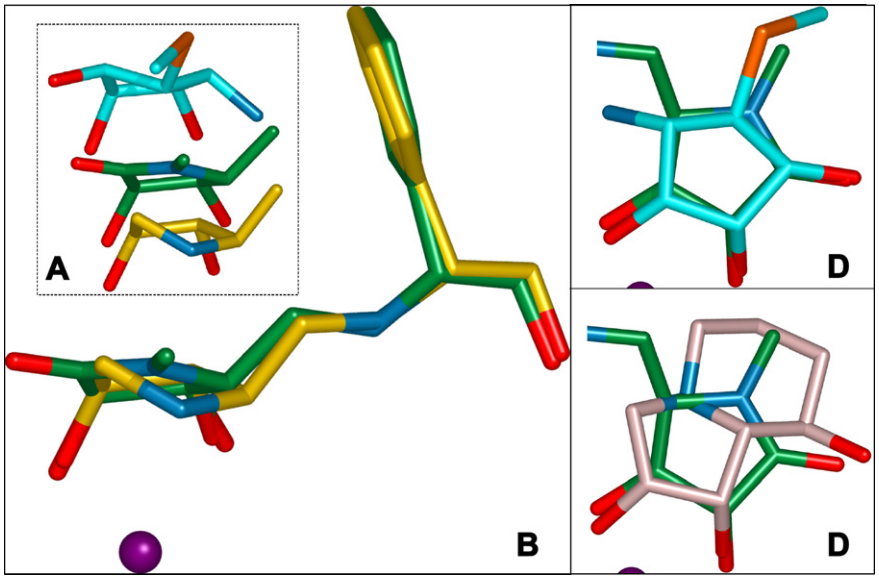

Figure 2. Overlays of **12** with previously solved inhibitors. Compounds are distinguished by coloring their carbons atoms green (**12**), yellow (**2**), cyan (mannostatin A) or light-pink (swainsonine). (A) Comparison of binding of **12** and **2** illustrates the change imposed by the introduction of the carbonyl. (B) Comparison with of the bound positions of mannostatin A and **12** shows that the binding of mannostatin A and the 5-membered ring of **12** is very similar. (C) The binding of swainsonine and the 5-membered ring of **12** is quite different although the oxygens end up in a very similar position. The insert panel **A** illustrates the differences in conformation of the 5-membered ring in **2**, **12** and mannostatin A. To obtain the overlays the complete protein:inhibitor complexes were superimposed using the SSM module of Coot and the coordinates for the zinc and inhibitor extracted. The active site zinc is colored magenta and is included as an aid to orientation.

Table 2
Inhibition by **1** (swainsonine) and compounds **2**, **3**, **11**, **12**, **13**, **14** of α-mannosidase activity extracted from human glioblastoma (LN18 and LNZ308) and endothelial (HCEC) cells

Compound	LNZ308	LN18	HCEC
	K_M = 650 μM	K_M = 1065 μM	K_M = 550 μM
1	IC_{50} = 20 nM	IC_{50} = 50 nM	IC_{50} = 10 nM
2	IC_{50} = 50 μM	IC_{50} = 50 μM	IC_{50} = 25 μM
	K_i = 41.5 μM	K_i = 32.5 μM	K_i = 23.3 μM
11	IC_{50} = 50 μM	IC_{50} = 350 μM	IC_{50} = 75 μM
12	IC_{50} = 500 nM	IC_{50} = 2 μM	IC_{50} = 500 nM
	K_i = 0.55 μM	K_i = 3.2 μM	K_i = 0.67 μM
3	IC_{50} = 75 μM	IC_{50} = 200 μM	IC_{50} = 75 μM
13	IC_{50} = 150 μM	IC_{50} = 750 μM	IC_{50} = 75 μM
14	IC_{50} = 7.5 μM	IC_{50} = 75 μM	IC_{50} = 750 nM

α-Mannosidase(s) were extracted at pH 5 from the LN18 and LNZ308 human glioblastoma cells or the human brain-derived HCEC endothelial cells and activity was measured using 4-methyl-umbelliferyl-α-mannopyranoside as substrate. K_M was determined first, then IC_{50} and K_i were determined in cell extracts pre-incubated for 30 min at 37 °C with increasing concentrations of the inhibitors under investigation. Then residual activity was measured using 4-methyl-umbelliferyl-α-mannopyranoside. K_M, IC_{50} and K_i values were determined graphically.

or not exposed to **14**, and found that more binding sites spanning a larger surface around the nucleus of tumor cells were detected in cells exposed than in cells not exposed to the inhibitor (Fig. 4). We also evaluated the incorporation by glioblastoma and proliferating endothelial cells of radioactive mannose compared to radioactive leucine into TCA-precipitable high molecular weight cellular molecules (Fig. 5a). The decrease of incorporation of mannose was higher than that of leucine in cells exposed to **14** (Fig. 5b) in LNZ308 and HCEC cells, but was less evident in LN18 cells. This difference is comparable to the lower K_i of inhibitor **12** (Fig. 5c) toward α-mannosidases II extracted from LNZ308 or HCEC cells than from LN18 cells.

3. Discussion

Two main classes of human α-mannosidases, types I and II, are involved in the processing of glycoproteins. Type I α(1,2)-mannosidases are localized in the endoplasmic reticulum, where their main functions are related to the quality control and correct folding of newly synthesized glycoproteins. These enzymes specifically hydrolyze α(1,2)mannosidic bonds of complex carbohydrate structures; they do not hydrolyze simple aryl-α-mannosides[42], and their enzymatic mechanisms and three-dimensional structures are different from those of α-mannosidases of type II. The type II α-mannosidases can be separated[33,43] into three groups: acidic/lysosomal (MAN2B1), intermediate/Golgi (GMII, MAN2A1), and neutral/cytosolic (MAN2C1/6A8). They have very similar sequences at their active sites and hydrolyze α(1,2), α(1,3), and α(1,6) linkages and simple aryl-α-mannosides by the same mechanism resulting in retention of sugar anomeric configuration. Increased expression of human lysosomal α-mannosidase II has been previously demonstrated in extracts of glioma, correlated with malignancy.[44] Human cytosolic α-mannosidase II is inhibited by swainsonine, and abrogation of its gene expression results in decreased growth of human nasopharyngeal tumor cells[45] and increased ConA binding in permeabilized fixed cells.[46] Golgi α-mannosidase II is inhibited by swainsonine with an IC_{50} = 20–50 nM. *Drosophila* GMII [47] displays 61% sequence identity with human GMII, comparable substrate specificity, kinetic properties, and inhibitor sensitivity,[28,48] and can be used as a valid model of the structural and functional features of the mammalian enzyme. Rose and co-workers analyzed a series of crystal structures of dGMII/inhibitor complexes[48–51] providing insight into the structure and catalytic mechanism of dGMII.

The crystallographic results presented here extend our work with pyrrolidine-based inhibitors and allow dissection of various aspects of their inhibitory properties. The first generation inhibitors[19,38] were unusual in that they lacked hydrogen bonds with Asp472 and Tyr727, as every previously solved structure displayed hydrogen bonding at this position. In these first generation structures, Asp472 and Tyr727 changed their orientation to allow formation of a hydrogen bond between them, causing a compression of this section of the active site.[38] It is probable that the binding energy from the T-shaped pi interaction between Trp95 and the phenyl ring of the inhibitor, another feature not pre-

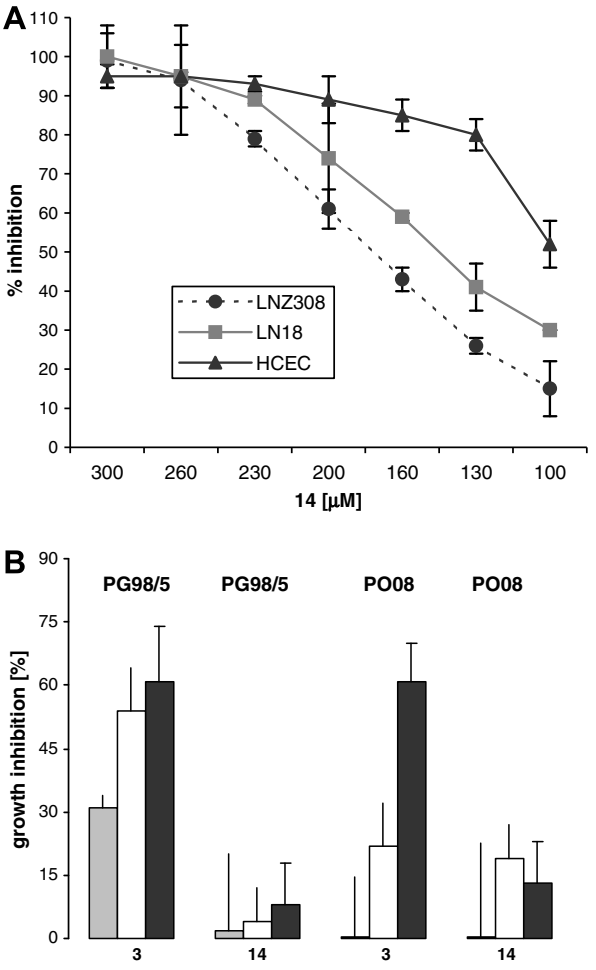

Figure 3. Cellular effects of cell-permeable α-mannosidase inhibitors in human glioblastoma cells, proliferating endothelial cells or fibroblasts. (A) Growth inhibition of human glioblastoma cells and proliferating endothelial cells. Human cells were exposed for 48 h to increasing concentrations of **14**, then the MTT assay was performed for the last 2 h and the percent of growth inhibition was calculated as the ratio of MTT reduction of treated to untreated cells. Results are shown as means ± SD of triplicate wells of one representative experiment out of 3. (B) Growth inhibition of human fibroblasts. Human primary dermal (PG98/5) or pulmonary (PO08) fibroblasts were exposed for 48 h to increasing concentrations of either **3** or **14**, then the MTT assay was performed for the last 2 h and the percent of growth inhibition was calculated as the ratio of MTT reduction of treated to untreated cells. Results are shown as means ± SD of triplicate wells. (grey bars: 100 μM; white bars: 200 μM; black bars: 300 μM).

viously seen in other inhibitors, was sufficient to overcome the unfavorable lack of hydrogen bonds.[38] The incorporation of an oxo group into the pyrrolidine ring, at the position similar to that of hydroxyl groups in other inhibitors, greatly increased the inhibitory efficiency of our second generation compounds and led to the formation of hydrogen bonds which were absent in the structures of the complexes of the first generation inhibitor. The Trp95:phenyl interactions are still maintained, and the position of the phenyl slightly differs between the first and second generation inhibitors. In the second generation inhibitors, the incorporation of the ketone group and the observed partial double bond character of the N1–C2 increased the rigidity of the pyrrolidine ring. This may be somewhat unfavorable to achieving potent inhibitory activity as we have previously demonstrated that the conformation of inhibitors bound to dGMII is quite distorted from their low energy conformation, and that inhibitors which more easily undergo conformational rearrangements are more potent.[40] An hydroxyl, rather than a carbonyl at C2 may produce a more effective inhibitor. A further improvement in the potency of the inhibitor came from the addition of the methyl group to the N1 nitrogen. The methyl group in compound **12** points toward a hydrophobic region, where we have previously seen binding of the thiomethyl group of mannostatin A and benzyl-mannostatin A.[40] In the case of the latter compound, the methyl was found directly in line with the end of Trp415. This hydrophobic interaction must be quite favorable for compound **12** as it is a better inhibitor than compound **11**, even though the presence of this methyl group caused the loss of a through-water hydrogen bond between Arg876 and N1. It is possible that the methyl group could be extended further to provide an even more potent inhibitor as there is still space available in the hydrophobic pocket. Thus, for dGMII, from a K_i value of 67 μM for our previous lead **2**,[19] our X-ray-based refinement of the inhibitor to obtain **12** resulted in a K_i value of 1 μM, thus a 67-fold gain in inhibition.

In human cancers, including glioblastoma, both the tumor cells themselves and the angiogenic endothelial cells associated with cancer may be targets of therapeutic intervention. Thus, we investigated the effects of our inhibitors in human LN18 and LNZ308 glioblastoma cells as models for tumor cells and human brain-derived HCEC endothelial cells as models for angiogenic endothelial cells associated with glioblastoma. The inhibition of α-mannosidase II activity by **11** and **12** was achieved in both cell types, suggesting that our inhibitors may be efficient in directly controlling tumor cell growth and also as potential anti-angiogenic molecules. Compared to the first generation inhibitor **2** and to **1** (swainsonine), **11** demonstrated a moderate inhibitory potency. Introduction of an oxo moiety at C(5) position of the five-membered ring did not result in significant modification of the inhibition of human α-mannosidases II extracted from human glioblastoma and endothelial cells. However, the *N*-methyl pyrrolidinone system **12** displayed potent inhibitory activity on human cell α-mannosidases, although lower than swainsonine. This result is in agreement with the observations made on the dGMII model enzyme. Interestingly, the inhibition of α-mannosidases II by **12**, but not **2** was more efficient in LNZ308 cells and HCEC cells than in LN18 cells, whereas inhibition by swainsonine was similar in all three cells. The growth inhibition of glioblastoma and endothelial cells only by the ester analogs **13** and **14** further confirms our previous hypothesis[19] that the transport across cell membrane of these inhibitors, and their subsequent intracellular trapping following hydrolysis of the ester moiety, is an important factor of their efficacy in human cells. The incorporation of mannose was reduced compared to leucine (a marker of general protein biosynthesis) in cells exposed to α-mannosidase inhibitor **14**. However, this effect was less evident in LN18 cells, which are less efficiently inhibited by **14** than LNZ308 and HCEC cells, strongly supporting a role for α-mannosidase II inhibition in the anti-growth effects of our inhibitor(s). Compound **14** was more potent than compound **13**, and slightly more potent than our previous lead **3**[19] in inhibiting the growth of human glioblastoma and endothelial cells. This did not reflect their potency in inhibiting α-mannosidase activity of cell extracts, but correlated with the potency of **11** and **12** at inhibiting the activity of our model enzyme dGMII. The derivatization of **11** and **12** into their 4-bromobenzoate esters induced a decrease of the inhibitory activity in cell extracts, as expected by the loss of interactions between the primary alcohol and residues of the active site of the enzyme. Still, the fact that a moderate amount of inhibition was observed suggests that the ester linkage was cleaved by cellular esterases to release the free primary alcohol. However, even if the growth inhibition of human tumor and tumor-associated endothelial cells was not improved by these modifications, their selectivity between human tumor-associated cells versus human normal fibroblasts was greatly enhanced.

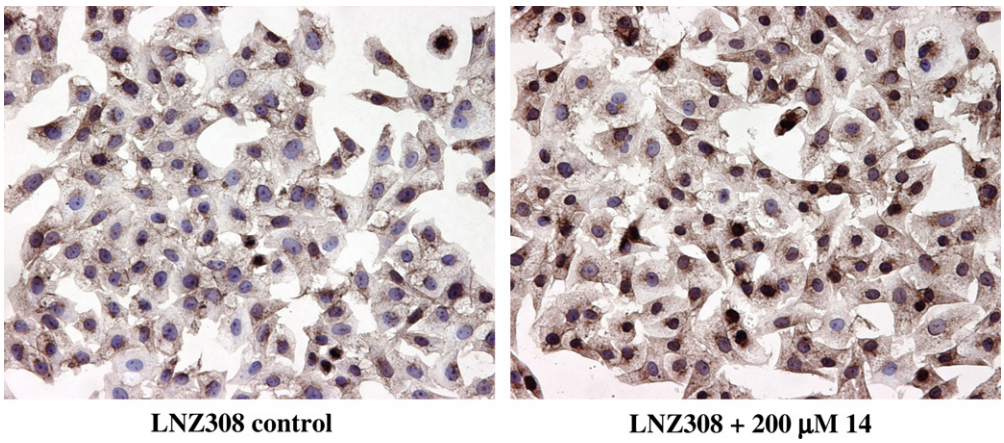

Figure 4. Lectin-cytochemistry of the human LNZ308 glioblastoma cells. LNZ308 cells were either not exposed (LNZ308 control) or exposed for 12 h to 200 µM **14** on histological slides. After fixation in buffered formol, the slides were exposed for 6 h to the α-D-mannopyranoside-specific lectin Lens culinaris (LcH). Co-incubation with the cognate lectin ligand, terminal α-D-mannopyranoside, demonstrated the absence of non-specific binding (not shown).

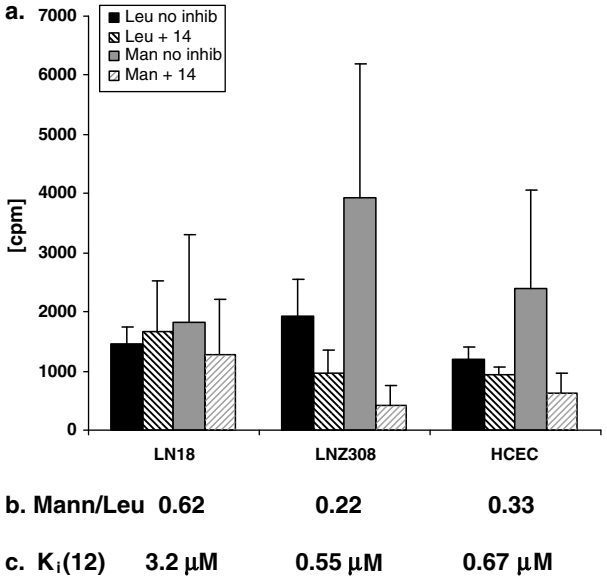

Figure 5. Inhibition of leucine (Leu) and Mannose (Mann) incorporation in human glioblastoma and endothelial cells by **14**. Human glioblastoma LN18 or LNZ308 cells were not exposed (no inhib) or exposed (+**14**) for 14 h to 200 µM **14** together with [^{3}H]-Leu (Leu) or [^{3}H]-Mann (Man), or human brain-derived HCEC endothelial cells were not exposed (no inhib) or exposed (+**14**) for 6 h to 200 µM **14** together with [^{3}H]-Leu or [^{3}H]-Mann. Then, (a) the incorporation of radioactivity by the cells into TCA-precipitable molecules was determined; (b) the ratio of the decrease of the incorporation of [^{3}H]-Mann to [^{3}H]-Leu in treated cell versus control cells was calculated (Man/Leu) and compared; and (c) to the K_i of the parent compound **12** for inhibition of mannosidase activity extracted from cells (from Table 2).

4. Conclusion

In summary, in the present manuscript, we describe the chemical syntheses, and enzymatic and biological characterization of congeners of inhibitors of α-mannosidase II. By refining the chemical structure using X-ray crystallography, we demonstrate an optimal fit of our lead molecules in the active site of Golgi α-mannosidase II. We also show that the inhibition of α-mannosidase II activity of human glioblastoma and angiogenic brain-derived endothelial cells and the inhibition of the growth of these cells in culture, while sparing healthy human fibroblasts, is achieved by these competitive inhibitors of α-mannosidases. Thus, the pyrrolidinone inhibitors of α-mannosidases II disclosed here constitute new promising scaffolds for the inhibition of human cellular α-mannosidase II and for a new class of future therapeutic drugs as anticancer and antiangiogenic agents.

5. Experimental

5.1. Chemical syntheses

Commercial reagents (Fluka, Aldrich) were used without purification. Solvents were filtered prior to use (Innovative Technology). Solutions after reactions and extractions were evaporated in a rotatory evaporator under reduced pressure. Reactions were monitored by TLC using Merck silica gel 60F_{254} plates, and detection by UV light, Pancaldi reagent [$(NH_4)_6MoO_4$, $Ce(SO_4)_2$, H_2SO_4, H_2O] or $KMnO_4$. Purification of compounds was performed by liquid/solid flash chromatography using silica gel (0.040–0.63 mm, Merck No.9385 silica gel 60, 240–400 mesh). The syntheses were performed as described in Scheme 2 and the detailed synthesis protocols and the characterization of the compounds are provided as Supplemental data.

5.2. Crystallography

Purified dGMII in Tris-buffer (10 mM Tris, pH 8.0, 150 mM NaCl) at a concentration of approximately 16 mg/ml was thawed and used for crystallization without any further treatment. Crystals of dGMII and complexes were grown using the hanging-drop vapor diffusion method using 1 ml of Tris-reservoir-buffer (0.1 M Tris, pH 7.0, 8.5% PEG 6K, 2.5% methyl-pentane diol (MPD)) in each well of the crystal tray. A total of 3 µl protein solution was combined with 3 µl crystal seeds in reservoir buffer to form the crystallization drop. Preparation of the seeds followed the Hampton protocol for the Seed Bead Kit. Seeds had been aliquoted at suitable concentrations and stored at −80 °C where they remain useable for at least 2 years. dGMII/inhibitor complexes were obtained either via co-crystallization or through soaking of a dGMII crystal in inhibitor solution. Co-crystals with **11** were obtained by incubating the enzyme on ice for 30 min with a final concentration of 2 mM **11** prior to crystallization. Crystals were grown for 16–18 h at 22 °C. They were removed from the drop using nylon CryoLoops (Hampton Research) and passed through Tris reservoir buffer containing increasing concentrations of MPD (10, 15, 20, 25%) for cryoprotection. Cryosolutions were also prepared containing inhibitor (1 mM final concentration). For soaking, dGMII crystals were first grown in Tris-buffer as described above. The next day, crystals were

washed in phosphate buffer (0.1 M sodium phosphate pH 7.0, 8.5% PEG 6K 2.5% MPD) followed by a 24-h soak in phosphate buffer containing 2 mM **12**. Crystals were then passed through phosphate buffer with 1 mM inhibitor containing increasing concentrations of MPD (10, 15, 20, 25% v/v) for cryoprotection. Crystals were flash frozen in a nitrogen stream.

5.3. Data collection of dGMII:11 and of dGMII:12 complexes

X-ray diffraction data for the dGMII:**11** complex were collected at 100 K on Beamline A1 at the Cornell High Energy Synchrotron Source. Data were integrated and scaled using HKL2000. A constant set of R_{free} data was created using CCP4[52] and by merging with a previous R_{free} data set. The data were then written in mtz, cns, and hklf4 formats for use in subsequent refinement programs. X-ray diffraction data for the dGMII:**12** complex were collected at 100 K with a Bruker X8 Proteum system consisting of a Bruker Microstar rotating anode generator, Montel optics, and a CCD detector. Data were integrated and scaled using the Proteum suite of programs.

5.4. Refinement of dGMII:11 and dGMII:12 complex structures

The structure of the dGMII:**11** complex was initially phased by molecular replacement using the software program CNS.[53] Rigid body refinement was carried out against the published structure of native dGMII (PDB:1HTY) with Tris and water molecules in the region of the active site removed. This was followed by simulated annealing to 3500 K, group B-factor refinement, and individual B-factor refinement. At this step, the R and R_{free} were 0.197 and 0.213 and the F_O–F_C density clearly revealed the presence of bound compound and unassigned water molecules. Additional water molecules were picked using the Arp/Warp[54] routine in CCP4. Ligand molecule dictionaries and starting coordinate files were generated using the ProDrg server (http://davapc1.bioch.dundee.ac.uk/programs/prodrg/). Ligand fitting and checking the model for proper fit to the density was performed using the program Coot.[55] At this stage, high resolution refinement using SHELX97[56] was started. CGLS refinement to increasing resolution was followed by refinement of anisotropic B-factors. This was followed by a number of iterative rounds of model building using Coot and SHELX97 refinement where clear alternative conformations of side chains were inserted into the model, water molecules were added and side chains were regularized. Hydrogen atoms were added and the occupancy of the alternative conformations was refined in later rounds of SHELX97 refinement. Statistics for data collection and refinement are presented in Supplemental Table S1. The model was prepared for PDB deposition using shelxpro, which removes the hydrogen atoms from the deposited molecule. The quality of the final model and ligand geometry were assessed using a number of structure validation programs including MolProbity (http://molprobity.biochem.duke.edu/), the Validation Suite (http://biotech.ebi.ac.uk), and hetze (http://xray.bmc.uu.se/hicup/). Simulated annealing omit maps were generated in CNS: the ligand was removed from the final model, the omit-model underwent a round of simulated annealing at 3500 K to remove any model bias in the phases, and $1F_{obs}$–F_{calc} and $2F_{obs}$–F_{calc} maps were generated. Protein overlays were carried out using the SSM module of Coot. Graphics were generated using Pymol (http://pymol.sourceforge.net) and Molscript (http://www.avatar.se/molscript/). The structure of the dGMII:**12** complex was initially solved by molecular replacement using CNS as described above. At this preliminary stage R and R_{free} were 0.17 and 0.21, respectively. Ligand, water fitting and alternate conformation assignment were as described above except that REFMAC was used for the final stages of refinement.

5.5. Cells and cell treatments

Human glioblastoma LN18 and LNZ308 (a kind gift of AC Diserens, Neurosurgery Department, CHUV, Lausanne, Switzerland) were grown in DMEM medium containing 4.5 g/l glucose, 5% FCS, and antibiotics.[41] HCEC cells are immortalized human brain-derived endothelial cells (a kind gift of D. Stanimirovic, Ottawa, Canada) and were grown in DMEM medium containing 4.5 g/l glucose, 10% FCS, and antibiotics.[14] PO08 and PG98/5 are human fibroblasts from the lungs and the skin, respectively, and were used as previously described.[19] All reagents for cell culture were from Gibco, (Invitrogen, Basel, Switzerland). Two days before experiments, cells were seeded in 48-well plates (Corning, NY, USA) in the same culture conditions. On the day of experiments medium was changed when indicated and cells were exposed to increasing concentrations of the synthetic derivatives for 24 h. Cell survival was determined using a MTT assay, essentially as previously described.[14,19,41] Briefly, MTT (3-(4,5-dimethyl-thiazol-2-yl)-2,5-diphenyl-tetrazolium bromide, Sigma, Switzerland) dissolved in PBS (5 mg/ml) was added to all wells without medium change, and the plates were incubated at 37 °C for 2 h. The precipitated formazan was dissolved in isopropanol–HCl and optical density measured at 540 nm. For the incorporation of [^{3}H]-Leu and [^{3}H]-Mann, LN18 and LNZ308 cells were seeded in 48-well plates for 10 h, then **14** (final concentration 200 μM) and [2,3,4,5-^{3}H]-L-Leu or [2,6-^{3}H]-D-Mann (both from American Radiolabeled Chemicals, St. Louis, MO, USA, final concentration 0.4 μCi/ml) were added for a further incubation of 14 h. Radioactivity incorporation was determined essentially as previously described.[19] Briefly, incorporation was quantified in a beta-counter (Rackbeta, LKB) after precipitation with 10% trichloracetic acid and solubilization in 0.1 N NaOH. Experiments were performed in triplicate wells and means ± SD were calculated.

5.6. Lectin labeling of human glioblastoma cells

Cells were grown on glass histological slides, exposed to inhibitors as indicated, fixed in buffered 4% formaldehyde and endogenous peroxidase was inactivated with 3% hydrogen peroxide in methanol. Slides were exposed overnight at 4 °C to biotin-labeled Lens culinaris lectin (LcH, Sigma L4143, stock solutions 1 mg/ml), diluted 1:2000 in antibody diluent (Dako, Baar, Switzerland) and subsequently exposed to avidin-complex (ABC, Dako) according to the manufacturer's instructions. Peroxidase activity was visualized using 0,035% diaminobenzidine (Fluka, Buchs, Switzerland) as a chromogen. Slides were conterstained with hematoxylin, and examined under a microscope. Co-incubation of the lectin on the slides with 0.1 M methyl-α-D-mannopyranoside (Fluka) was used as control for specific binding of the lectin (not shown).

5.7. Evaluation of inhibitory activity on α-mannosidase from jack bean

Determination of the activity of α-mannosidase from jack bean was performed according to published protocols.[57] Briefly, 0.01 to 0.5 U/mL of jack bean α-mannosidase (Sigma), preincubated for 5 min at 20 °C with the inhibitor under evaluation, was incubated for 20 min at 37 °C with increasing concentrations of 4-nitrophenyl-α-D-manno-pyranoside (Sigma) buffered to pH 5.5 (optimal pH of the enzyme). The reaction was stopped by addition of 2.5 volume of 0.2 M sodium borate buffer pH 9.8. The 4-nitrophenolate formed was quantified at 410 nm and either IC_{50} values were determined graphically or double-reciprocal (Lineweaver and Burk) plots were used to determine the inhibition characteristics.

5.8. Evaluation of inhibitory activity on dGMII

For the determination of K_i values for the inhibition of dGMII, aliquots of dGMII were diluted to 5 μg/ml in 10 mM sodium phosphate, pH 6.8, 100 mM NaCl, and 10 μg/ml bovine serum albumin. Inhibitor dissolved in DMSO was added and incubated with the enzyme for 30 min at 20 °C. The reaction was initiated by the addition of para-nitrophenyl α-manno-pyranoside (Fluka) dissolved in DMSO, and the incubation was done at 20 °C. The final concentration of DMSO in all cases was 10%. Aliquots were removed at various time points, put into a microtitre plate, and an equal volume of 0.5 M sodium carbonate was added to stop the reaction. Absorbance at 405 nm was measured in a microplate reader (Molecular Devices). The linear portion of the reaction time course was used to determine inhibition constants. The anemona.xlt Excel spreadsheet[58] was used for determination of K_i values using nonlinear regression analysis.

5.9. Evaluation of cellular α-mannosidase activity and inhibition

Human cell layers were extracted in phosphate buffers containing 0.1% Triton X-100 (Fluka) pH 5.0, and incubated at room temperature for 10–30 min in the absence or presence of the synthetic inhibitors at the concentration indicated. The activity of α-mannosidase(s) was determined by the addition of the fluorigenic substrate 4-methyl-umbelliferyl-α-D-manno-pyranoside (Fluka, final concentration 150 μM) by measuring the fluorescence increase for 30 min in a fluorescence multiwell plate reader (Cytofluor, PerSeptive BioSystems) thermostated at 37 °C, λ_{ex} = 360 nm; λ_{em} = 460 nm, essentially as previously described.[19] Swainsonine (Fluka) was used as a reference inhibitor.

5.10. Calculations of results

Each experiment was repeated in triplicate wells at least three times. Means and standard deviation were calculated.

Acknowledgments

We thank Ms. Catherine Chapuis Bernasconi, Solange Gros, Sylviane Trepey, Mr. Martial Rey, Alain Razaname, and Francisco Sepulveda for excellent technical help and the CHESS synchrotron facility for beam time. This work is based upon research conducted at the Cornell High Energy Synchrotron Source (CHESS), which is supported by the National Science Foundation under award DMR-0225180, using the Macromolecular Diffraction at CHESS (MacCHESS) facility, which is supported by award RR-01646 from the National Institutes of Health, through its National Center for Research Resources. We also thank the Swiss National Foundation (Grant No. 200020-100028/ 1), the Swiss League against cancer (Grant No. KLS-01308-02-2003), and the Canadian Institutes of Health Research (Grants 42452 and 79312) for financial support.

Supplementary data

Supplementary Table S1: Statistics for data collection and refinement of dGMII in complex with **11** or **12**, Table S2: Interatomic distances in the crystal structure, and Table S3: Inhibition of cell growth of human glioblastoma (LN18 and LNZ308) and endothelial (HCEC) cells by functionalized pyrrolidinones. Supplemental Figure S1: Interaction of **2** with residues in the active site of dGMII. Experimental synthesis procedures and characterization of the compounds **4**, **5**, **6**, **7**, **9**, **10**, **11**, **12**, **13**, and **14**. Supplementary data associated with this article can be found, in the online version, at doi:10.1016/j.bmc.2008.06.021.

References and notes

1. Dennis, J. W.; Granovski, M.; Warren, C. E. *BioEssays* **1999**, *21*, 412.
2. Helenius, A.; Aebi, M. *Ann. Rev. Biochem.* **2004**, *73*, 1019.
3. Jacob, G. S. *Curr. Opin. Struct. Biol.* **1995**, *5*, 605.
4. Bernacki, R. J.; Niedbala, M. J.; Korytnyk, W. *Cancer Meta Rev.* **1985**, *4*, 81.
5. Dube, D. H.; Bertozzi, C. R. *Nat. Rev. Drug Discov.* **2005**, *4*, 477.
6. Hakomori, S. *Proc. Nat. Acad. Sci. U.S.A.* **2002**, *99*, 10231.
7. Dennis, J. W.; Granovsky, M.; Warren, C. E. *Biochim. Biophys. Acta* **1999**, *1473*, 21.
8. Scanlin, T. F.; Glick, M. C. *Glycoconjugate J.* **2000**, *17*, 617.
9. Liu, F. T.; Rabinovich, G. A. *Nat. Rev. Cancer* **2005**, *5*, 29.
10. Fuster, M. M.; Esko, J. D. *Nat. Rev. Cancer* **2005**, *5*, 526.
11. Gerber-Lemaire, S.; Juillerat-Jeanneret, L. *Mini Rev. Med. Chem.* **2006**, *6*, 1043.
12. Winchester, B. *Glycobiology* **2005**, *15*, 1R.
13. Ito, Y.; Hagihara, S.; Matsuo, I.; Totani, K. *Curr. Opin. Struct. Biol.* **2005**, *15*, 481.
14. Hanessian, S.; Zhan, L.; Bovey, R.; Saavedra, O. M.; Juillerat-Jeanneret, L. *J. Med. Chem.* **2003**, *46*, 3600.
15. Gerber-Lemaire, S.; Popowycz, F.; Rodriguez-Garcia, E.; Carmona Asenjo, A. T.; Robina, I.; Vogel, P. *ChemBioChem* **2002**, *5*, 466.
16. Popowycz, F.; Gerber-Lemaire, S.; Demange, R.; Rodriguez-Garcia, E.; Carmona Asenjo, A. T.; Robina, I.; Vogel, P. *Bioorg. Med. Chem. Lett.* **2001**, *11*, 2489.
17. Popowycz, F.; Gerber-Lemaire, S.; Rodriguez-García, E.; Schütz, C.; Vogel, P. *Helv. Chim. Acta* **2003**, *86*, 1914.
18. Popowycz, F.; Gerber-Lemaire, S.; Schütz, C.; Vogel, P. *Helv. Chim. Acta* **2004**, *87*, 800.
19. Fiaux, H.; Popowycz, F.; Favre, S.; Schütz, C.; Vogel, P.; Gerber-Lemaire, S.; Juillerat-Jeanneret, L. *J. Med. Chem.* **2005**, *48*, 4237.
20. Fiaux, H.; Schütz, C.; Vogel, P.; Gerber-Lemaire, S.; Juillerat-Jeanneret, L. *Chimia* **2006**, *60*, 185.
21. Favre, S.; Fiaux, H.; Schütz, C.; Vogel, P.; Juillerat-Jeanneret, L.; Gerber-Lemaire, S. *Heterocycles* **2006**, *69*, 179.
22. Lillelund, V. H.; Jensen, H. H.; Liang, X.; Bols, M. *Chem. Rev.* **2002**, *102*, 515.
23. Olden, K.; Breton, P.; Grzegorzewski, K.; Yasuda, Y.; Gause, B. L.; Oredipe, O. A.; Newton, S. A.; White, S. L. *Pharmacol. Ther.* **1991**, *50*, 285.
24. Asano, N.; Nash, R. J.; Molyneux, R. J.; Fleet, G. W. J. *Tetrahedron Asymetr.* **2000**, *11*, 1645.
25. Asano, N. *Glycobiology* **2003**, *13*, 93R.
26. Colegate, S. M.; Dorling, P. R.; Huxtable, C. R. *Austr. J. Chem.* **1979**, *32*, 2257.
27. Yeo, T. K.; Yeo, K. T.; Parent, J. B.; Olden, K. *J. Biol. Chem.* **1985**, *260*, 2565.
28. Przybylo, M.; Litynska, A.; Poche, E. *Biochimie* **2005**, *87*, 133.
29. Humphries, M. J.; Matsumoto, K.; White, S. L.; Olden, K. *Proc. Natl. Acad. Sci. U.S.A.* **1986**, *83*, 1752.
30. Kino, T.; Inamura, N.; Nakahara, H.; Kiyoto, K.; Goto, T.; Terano, H.; Kohsaka, M.; Aoki, H.; Imanaka, H. *J. Antibiot.* **1995**, *38*, 936.
31. Goss, P. E.; Reid, C. L.; Bailey, D.; Dennis, J. W. *Clin. Cancer Res.* **1997**, *3*, 1077.
32. Dwek, R. A.; Butters, T. D.; Platt, F. M.; Zitzmann, N. *Nat. Rev. Drug Discov.* **2002**, *1*, 65.
33. Dwek, M. V.; Brooks, S. A. *Curr. Cancer Drug Target* **2004**, *4*, 425.
34. Hembre, E. J.; Pearson, W. H. *Tetrahedron* **1997**, *53*, 11021.
35. Pearson, W. H.; Hembre, E. J. *J. Org. Chem.* **1996**, *61*, 5537.
36. Pearson, W. H.; Guo, L. *Tetrahedron Lett.* **2001**, *42*, 8267.
37. Pearson, W. H.; Hembre, E. J. *Tetrahedron Lett.* **2001**, *42*, 8273.
38. Englebienne, P.; Fiaux, H.; Kuntz, D. A.; Corbeil, C. R.; Gerber-Lemaire, S.; Kuntz, D. A.; Rose, D. R.; Moitessier, N. *Proteins* **2007**, *69*, 160.
39. Ikota, N.; Nakagawa, H.; Ohno, S.; Noguchi, K.; Okuyama, K. *Tetrahedron* **1998**, *54*, 8985.
40. Kawatkar, S. P.; Kuntz, D. A.; Woods, R. J.; Rose, D. R.; Boons, G. J. *J. Am. Chem. Soc.* **2006**, *128*, 8310.
41. Juillerat-Jeanneret, L.; Célérier, J.; Chapuis Bernasconi, C.; Nguyen, G.; Wostl, W.; Maerki, H. P.; Janzer, R. C.; Corvol, P.; Gasc, J. M. *Br. J. Cancer* **2004**, *90*, 1059.
42. Vasella, A.; Davies, G. J.; Böhm, M. *Curr. Opin. Chem. Biol.* **2002**, *6*, 619.
43. Daniel, P. F.; Winchester, B.; Warren, C. D. *Glycobiology* **1994**, *4*, 551.
44. Wielgat, P.; Walczuk, U.; Szajda, S.; Bien, M.; Zimmoch, L.; Mariak, Z.; Zwier, K. J. *Neurooncology* **2006**, *80*, 243.
45. Yue, W.; Jin, Y. L.; Shi, G. X.; Liu, Y.; Gao, Y.; Zhao, Y.; Zhu, L. *Int. J. Cancer* **2004**, *108*, 189.
46. Yanagida, K.; Natsuka, S.; Hase, S. *Glycobiology* **2006**, *16*, 294.
47. Rabouille, C.; Kuntz, D. A.; Lockyer, A.; Watson, R.; Signorelli, T.; Rose, D. R.; van den Heuvel, M.; Roberts, D. B. *J. Cell Sci.* **1999**, *112*, 3319.
48. van den Elsen, J. M. H.; Kuntz, D. A.; Rose, D. R. *EMBO J.* **2001**, *20*, 3008.
49. Kuntz, D. A.; Ghavami, A.; Johnston, B. D.; Pinto, B. M.; Rose, D. R. *Tetrahedron Asymmetr.* **2005**, *16*, 25.
50. Numao, S.; Kuntz, D. A.; Withers, S. G.; Rose, D. R. *J. Biol. Chem.* **2003**, *278*, 48074.
51. Rose, D. R.; Kuntz, D. A.; van den Elsen, J. M. H. *US Pat. Appl. Publ. US.* **2002**, 172670
52. Collaborative Computational Project, Number 4. *Acta Cryst.* **1994**, *D50*, 760.
53. Brunger, A. T.; Adams, P. D.; Clore, G. M.; Delano, W. L.; Gros, P.; Grosse-Kunstleve, R. W.; Jiang, J. S.; Kuszewski, J.; Nilges, M.; Pannu, N. S.; Read, R. J.; Rice, L. M.; Simonson, T.; Warren, G. L. *Acta Cryst.* **1998**, *D54*, 905.

54. Lamzin, V. S.; Perrakis, A.; Wilson, K. S. In *The ARP/WARP Suite for Automated Construction and Refinement of Protein Models. Int. Tables for Crystallography. Vol. F: Crystallography of Biological Macromolecules*; Rossmann, M. G., Arnold, E., Eds.; Dordrecht, Kluwer Academic Publishers: The Netherlands, 2001; pp 720–722.
55. Emsley, P.; Cowtan, K. *Acta Cryst.* **2004**, *D60*, 2126.
56. Sheldrick, G. M.; Schneider, T. R. *Methods Enzymol.* **1997**, *277*, 319.
57. Brandi, A.; Cicchi, S.; Cordero, F. M.; Frignoli, B.; Goti, A.; Picasso, S.; Vogel, P. *J. Org. Chem.* **1995**, *60*, 6806.
58. Hernández, A.; Ruiz, M. T. *Bioinformatics* **1998**, *14*, 227.